ROYAL SOCIETY OF CHEMISTRY

PAPER

View Article Online
View Journal | View Issue

Fluorescent sensing and selective adsorption properties of metal–organic frameworks with mixed tricarboxylate and 1*H*-imidazol-4-yl-containing ligands†

Zhi-Qiang Liu,[a] Yue Zhao,[a] Peng Wang,[a] Yan-Shang Kang,[a] Mohammad Azam,[b] Saud I. Al-Resayes,[b] Xiao-Hui Liu,[a] Qing-Yi Lu[a] and Wei-Yin Sun (ID) *[a]

Herein, two metal–organic frameworks (MOFs), $[Co_4(\mu_3\text{-OH})_2(L)(BTB)_2(H_2O)_3]\cdot5.6H_2O$ (**1**) and $[Cd_3(L)_2(BTB)_2(\mu_2\text{-}H_2O)]\cdot7.4H_2O$ (**2**), based on 1,3-di(1*H*-imidazol-4-yl)benzene (L) and 1,3,5-tri(4-carboxyphenyl)benzene (H_3BTB), respectively, have been achieved. Compound **1** is a porous three-dimensional (3D) framework with butterfly-like tetranuclear clusters as 7-connected nodes, and compund **2** is a 3D net with a different topology. Remarkably, compounds **1** and **2** exhibit selective adsorption of CO_2 over N_2 and methyl orange (MO) dye molecules. Magnetic measurements reveal that there are antiferromagnetic interactions within the tetranuclear cluster in **1**. Furthermore, **2** was well-dispersed in different solvents, and their luminescent properties were investigated, and the results indicated that **2** could be considered as a potential luminescent probe for the detection of ketone molecules.

Introduction

During the past few years, metal–organic frameworks (MOFs) have attracted significant interest not only due to their interesting structures and topologies but also owing to their diversified structure-based functions such as gas storage and separation, magnetism, luminescence, ion exchange, molecular recognition, and catalysis.[1] Among these, MOFs with magnetic interactions, especially those displaying long-range ordering, are considered to be candidates for multifunctional molecular materials. It has been reported that spin carrying units such as paddlewheel $[M_2(CO_2)_4]$ and trinuclear $[M_3O(CO_2)_6]$ clusters can be used as secondary building units (SBUs) for the fabrication of porous magnets.[2] In addition, MOFs have the potential for CO_2 adsorption and separation because of their structural diversities and functionalities, such as high surface area, tunable pore sizes and shapes, as well as modifiable surface properties. Gas separation, including selective adsorption of

CO_2 from industrial and natural gases, becomes highly important from the aspect of energy and environment for the future.[3] Furthermore, fluorescence based on luminescent MOFs shows remarkable promise owing to the short response time, high sensitivity, simplicity, as well as low-cost of the luminescent MOFs. Varied fluorescent MOFs have been developed with a promising sensing ability towards ketone molecules, explosives, and metal ions through fluorescence quenching or enhancement effect.[4] Although significant progress has been achieved in this field over the past few years, it is still a great challenge for us to fabricate MOFs with definite structures and functions because there are varied factors that can affect the structures and properties of the MOFs.[5] Obviously, the design and choice of organic ligands is a crucial step in the construction of desired MOFs. For instance, multitopic organic ligands with 1-imidazole moieties have been intensively used in the construction of MOFs.[6–8] Compared with these well-used 1-imidazole-containing ligands, 4-imidazole-based compounds can act as both anionic and neutral ligands with and without the deprotonation of the NH group, and as a result, can exhibit more versatile coordination modes in the formation of MOFs;[9–11] however, MOFs with 4-imidazole-containing ligands have not been well-documented to date. Therefore, in this study, we employed a rigid 4-imidazole-based ligand, 1,3-di(1*H*-imidazol-4-yl)benzene (L).

On the other hand, mixed organic ligands, particularly the combination of multicarboxylate and N-donor ligands, have been demonstrated to be a powerful approach for the fabrica-

[a]Coordination Chemistry Institute, State Key Laboratory of Coordination Chemistry, School of Chemistry and Chemical Engineering, Nanjing National Laboratory of Microstructures, Collaborative Innovation Center of Advanced Microstructures, Nanjing University, Nanjing 210023, China. E-mail: sunwy@nju.edu.cn; Tel: +86 25 89683485
[b]Department of Chemistry, College of Science, King Saud University, P. O. Box 2455, Riyadh 11451, Kingdom of Saudi Arabia

†Electronic supplementary information (ESI) available: XRD, TG and additional figures. CCDC 1538508 and 1538509. For ESI and crystallographic data in CIF or other electronic format see DOI: 10.1039/c7dt01759f

tion of novel MOFs because of their strong coordination ability and varied coordination modes.[11] Herein, we focused our attention on the reactions of mixed organic ligands of L and 1,3,5-tri(4-carboxyphenyl)benzene (H_3BTB) with Co(II) and Cd(II) salts, and two new MOFs, $[Co_4(\mu_3\text{-OH})_2(L)(BTB)_2(H_2O)_3]\cdot 5.6H_2O$ (**1**) and $[Cd_3(L)_2(BTB)_2(\mu_2\text{-}H_2O)]\cdot 7.4H_2O$ (**2**), were successfully synthesized. They were characterized *via* X-ray crystallography and thermal and elemental analyses. Selective adsorption and luminescent sensing properties of **1** and **2** were investigated.

Experimental

Materials and methods

All commercially available chemicals and solvents were of reagent grade and were used as received. Ligand L was synthesized according to the previously reported procedures.[12] Elemental analyses for C, H, and N were performed using an Elementar Vario MICRO elemental analyzer. FTIR spectral measurements were carried out *via* a Bruker Vector 22 FTIR spectrophotometer using KBr pellets. Thermogravimetric analyses (TGA) were performed using a Mettler-Toledo (TGA/DSC1) thermal analyzer under nitrogen at a heating rate of 10 °C min^{-1}. Powder X-ray diffraction (PXRD) analyses were carried out *via* a Bruker D8 Advance using Cu Kα radiation (λ = 1.5418 Å) with the X-ray tube operated at 40 mA and 40 kV. Sorption data were obtained using a Belsorp-max volumetric gas sorption instrument. UV-vis spectra were obtained using a UVProbe 2.33 spectrophotometer. The luminescence spectra were obtained using an Aminco Bowman Series 2 spectrofluorometer with a xenon arc lamp as the light source. The pass width of 10 nm was used in the measurements of the emission and excitation spectra, and all the measurements were performed under the same experimental conditions. Magnetic measurements over the temperature range of 2–300 K were carried out using a Quantum Design MPMS 5 SQUID magnetometer.

Synthesis of $[Co_4(\mu_3\text{-OH})_2(L)(BTB)_2(H_2O)_3]\cdot 5.6H_2O$ (1). A mixture of L (21.0 mg, 0.10 mmol), $CoSO_4\cdot 7H_2O$ (56.2 mg, 0.20 mmol), H_3BTB (43.8 mg, 0.10 mmol), and NaOH (12.0 mg, 0.3 mmol) in a CH_3OH/H_2O (1:3) solution (10 ml) was sealed in a Teflon-lined stainless steel container and heated at 120 °C for 3 days. After being cooled down to room temperature, pink block crystals of **1** were obtained in 72% yield based on H_3BTB. Anal. calcd for $C_{66}H_{59.2}N_4O_{22.6}Co_4$: C, 52.65; H, 3.96; N, 3.72%. Found: C, 52.76; H, 3.99; N, 3.74%. IR (KBr pellet, cm^{-1}): 3405 (m), 1656 (s), 1589 (s), 1402 (s), 1186 (w), 1125 (w), 1014 (w), 960 (w), 811 (m), 747 (s), 712 (m), 672 (w), 643 (w), 475 (w).

Synthesis of $[Cd_3(L)_2(BTB)_2(\mu_2\text{-}H_2O)]\cdot 7.4H_2O$ (2). A mixture of L (21.0 mg, 0.10 mmol), $Cd(NO_3)_2\cdot 4H_2O$ (61.7 mg, 0.20 mmol), and H_3BTB (43.8 mg, 0.10 mmol) in DMF/H_2O (1:1) solution (10 ml) was sealed in a Teflon-lined stainless steel container and heated at 120 °C for 3 days. After being cooled down to room temperature, colorless block crystals of **2**

were obtained in 52% yield based on H_3BTB. Anal. calcd for $C_{78}H_{65.8}N_8O_{20.4}Cd_3$: C, 52.67; H, 3.73; N, 6.30%. Found: C, 52.81; H, 3.68; N, 6.32%. IR (KBr pellet, cm^{-1}): 3422 (m), 3131 (m), 1654 (s), 1582 (s), 1394 (s), 1183 (w), 1108 (w), 1078 (w), 961 (w), 817 (m), 746 (s), 707 (m), 669 (w), 623 (w), 473 (w).

Sample activation. Solvent-exchanged sample was prepared by immersing the as-synthesized sample **1** or **2** in acetone for 3 days to remove the nonvolatile solvates; the solvent was decanted every 12 h and fresh acetone was added. The activated samples **1′** and **2′** were obtained by heating the solvent-exchanged samples at 358 K under a dynamic high vacuum for 10 h.

X-ray crystallography

Diffraction data collections for **1** and **2** were conducted using a Bruker Smart Apex II CCD area-detector diffractometer with graphite-monochromated Mo Kα radiation (λ = 0.71073 Å). The integration of the diffraction data as well as the intensity corrections for the Lorentz and polarization effects were carried out using the SAINT program.[13] Semi-empirical absorption correction was performed using the SADABS program.[14] The structures of **1** and **2** were solved *via* direct methods using SHELXS-2014, and all the non-hydrogen atoms were anisotropically refined on F^2 by the full-matrix least-squares technique using SHELXL-2014.[15] The hydrogen atoms, except for those of water molecules, were geometrically generated and isotropically refined using the riding model. Atoms C61, C62, and C63 and C73, C74, and C75 in **2** are disordered at two positions with the site occupancies of 0.62(4) and 0.38(4) for C61, C62, and C63, and 0.68(2) and 0.32(2) for C73, C74, and C75. Because the guest solvent molecules in **1** and **2** are highly disordered and impossible to refine using the conventional discrete-atom models, the SQUEEZE subroutine of the PLATON software suite was used to remove the scattering from the highly disordered solvent molecules.[16] The formulae of **1** and **2** were obtained based on the volume/count_electron analysis and TG and elemental analyses. The reported refinements are of the guest-free structures obtained by the SQUEEZE routine, and the results are attached to the CIF file. The details of the crystal data for **1** and **2** are summarized in Table 1, and the selected bond lengths and angles are listed in Table S1 (ESI†).

## Results and discussion

Crystal structure description

Crystal structure of $[Co_4(\mu_3\text{-OH})_2(L)(BTB)_2(H_2O)_3]\cdot 5.6H_2O$ (1). The results of the single crystal X-ray structural analysis show that **1** crystallizes in the triclinic space group $P\bar{1}$, and there are four crystallographically independent Co(II) atoms, two μ_3-OH, one L, two completely deprotonated BTB^{3-}, and three coordinated water molecules in the asymmetric unit of **1**. As exhibited in Fig. 1a and b, **1** contains a tetranuclear cluster $[Co_4(\mu_3\text{-OH})_2]$ bridging linked by two OH$^-$ groups that can be considered as an SBU. Co1 and Co3 have the same four coordi-

Table 1 Crystal data and structure refinements for **1** and **2**

	1	2
Empirical formula	$C_{66}H_{59.2}N_4O_{22.6}Co_4$	$C_{78}H_{65.8}N_8O_{20.4}Cd_3$
Formula weight	1505.72	1778.81
Crystal system	Triclinic	Monoclinic
Space group	$P\bar{1}$	$P2_1/c$
a (Å)	15.082(3)	15.5620(9)
b (Å)	16.887(3)	32.1384(18)
c (Å)	17.338(3)	14.8953(8)
α (°)	114.224(4)	90
β (°)	102.313(4)	91.9120(10)
γ (°)	100.882(4)	90
V (Å^3)	3740.4(11)	7445.6(7)
Z	2	4
D_c (g cm^{-3})	1.247	1.468
μ (mm^{-1})	0.934	0.916
F (000)	1432	3296
Reflections collected	22 686	41 131
Unique reflections	12 806	13 038
Goodness-of-fit	1.025	1.033
R_1 [a] $[I > 2\sigma(I)]$	0.0818	0.0346
wR_2 [b] $[I > 2\sigma(I)]$	0.2424	0.0842

[a] $R_1 = \sum ||F_o| - |F_c||/\sum |F_o|$. [b] $wR_2 = |\sum w(|F_o|^2 - |F_c|^2)|/\sum |w(F_o)^2|^{1/2}$, where $w = 1/[\sigma^2(F_o^2) + (aP)^2 + bP]$. $P = (F_o^2 + 2F_c^2)/3$.

nation numbers with a distorted tetrahedral coordination geometry, but different coordination environments. Co1 is coordinated by three carboxylate oxygen atoms (O2, O6A, and O7) from three different BTB^{3-} ligands and one μ_3-OH oxygen one (O13), whereas Co3 is surrounded by two carboxylate oxygen atoms (O9C and O11D) from two distinct BTB^{3-} ligands, one imidazole nitrogen (N4E), and one μ_3-OH oxygen (O16). Both Co2 and Co4 with distorted octahedral coordination geometry are six coordinated with different coordination donor sets. Co2 is coordinated by one imidazole nitrogen (N1) from one L, two carboxylate oxygen atoms (O4B and O10C) from two different BTB^{3-} ligands, two μ_3-OH oxygen atoms (O13 and O16), and one coordinated aqua molecule (O17), whereas Co4 is coordinated by two μ_3-OH oxygen atoms (O13 and O16), two carboxylate oxygen atoms (O3B and O5A) from two distinct BTB^{3-} ligands, and two coordinated aqua molecules (O14 and O15). Each tetranuclear cluster in **1** has the common {M$_4$O$_2$} butterfly motif, with μ_3-OH oxygen atoms (O13 and O16) linking the wing-tip cobalt centers (Co1 and Co3) to the body cobalt centers (Co2 and Co4). Note that the BTB^{3-} ligands in **1** present two different coordination modes, as shown in Fig. S1a and S1b (ESI†): one is $(\mu_1-\eta^1:\eta^0)$-$(\mu_1-\eta^1:\eta^0)$-$(\mu_2-\eta^1:\eta^1)$-BTB tetradentate coordination mode that connects four Co(II) atoms and another one adopts a μ_5-bridging mode to link five Co(II) atoms with its three carboxylate groups in the $(\mu_1-\eta^1:\eta^0)$-$(\mu_2-\eta^1:\eta^1)$-$(\mu_2-\eta^1:\eta^1)$-BTB pentadentate coordination mode. The ligands BTB^{3-} link Co(II) atoms to form a three-dimensional (3D) architecture with a large cavity (Fig. 1c). Furthermore, L ligands filled into the Co(II)–BTB 3D framework *via* Co–N coordination interactions to provide the eventual 3D architecture of **1** (Fig. 1d). PLATON calculation suggests that the free volume after the removal of free water molecules is 26.7%.[17]
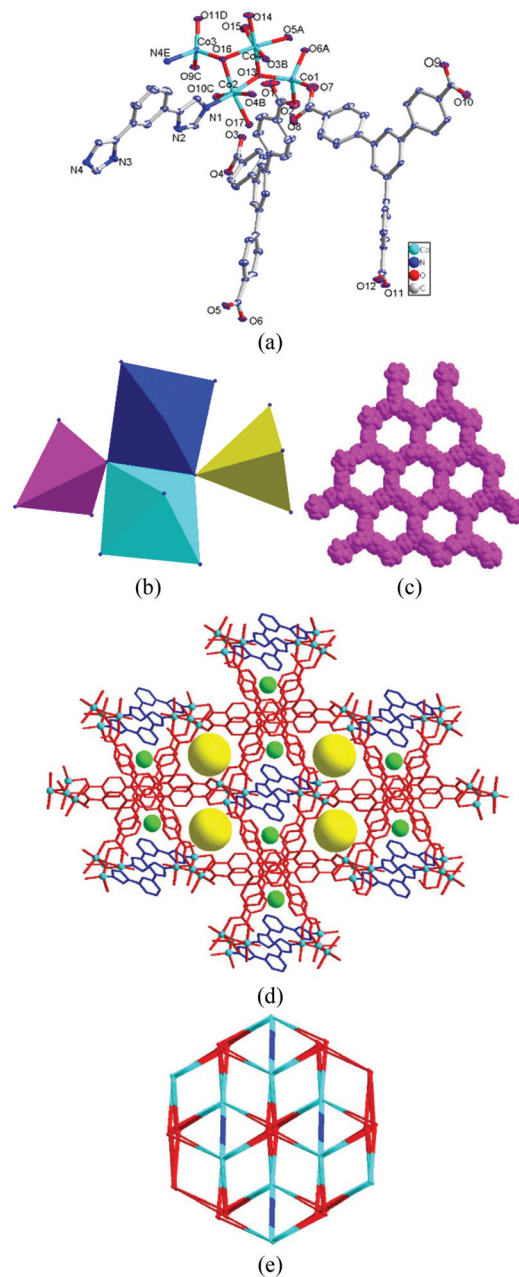
Fig. 1 (a) Coordination environment of Co(II) in **1** with ellipsoids drawn at the 30% probability level. Hydrogen atoms and free solvent molecules are omitted for clarity. (b) Tetranuclear SBU [Co$_4$(μ_3-OH)$_2$] in **1**. (c) 3D framework of Co(II)–BTB^{3-}. (d) 3D framework of **1** (e) topology of **1** (turquoise: Co$_4$(μ_3-OH)$_2$ SBU, red: BTB^{3-} ligand; and blue: L ligand).

To simplify the 3D structure of **1**, topological analysis was performed. As illustrated in Fig. S2a (ESI†), each [Co$_4$(μ_3-OH)$_2$] SBU is surrounded by six BTB^{3-} and two L ligands; however, two L link two [Co$_4$(μ_3-OH)$_2$] SBUs and accordingly can be viewed as a single-connector. Therefore, each [Co$_4$(μ_3-OH)$_2$] SBU can be regarded as a seven-connector. On the other hand, each BTB^{3-} ligand connects three [Co$_4$(μ_3-OH)$_2$] SBUs and can be considered as a three-connector. Thus, the resulting structure of **1** can be simplified as an unusual (3, 7)-connected

bi-nodal 3D net, with the point (Schläfli) symbol of $\{4\cdot6^2\}_2\{4^2\cdot6^{16}\cdot8^3\}$ (Fig. 1e). Compound **1** is the first example of a porous 3D topological framework with butterfly-like tetra-nuclear clusters as 7-connected nodes.

Crystal structure of $[Cd_3(L)_2(BTB)_2(\mu_2\text{-}H_2O)]\cdot7.4H_2O$ (2). When aqueous DMF solution was used as the reaction medium, a cadmium complex **2** was obtained. Crystal structural analysis revealed that **2** crystallizes in the monoclinic space group $P2_1/c$, which is different from that obtained from the reaction with the addition of NaOH.[4b] There are three crystallographically independent Cd(II) atoms in the repeating unit of **2**, as illustrated in Fig. 2a, and Cd1, Cd2, and Cd3 atoms have similar coordination environments and geometries with those in the previously reported framework.[4b] There are weak interactions between Cd3 and O6 as well as Cd3 and O7 since the distances of Cd–O6 and Cd–O7 are 2.647(3) and 2.635 (3), respectively. BTB^{3-} ligands in the framework **2** also display two different coordination modes: $(\mu_1\text{-}\eta^1\text{:}\eta^0)\text{-}(\mu_1\text{-}\eta^1\text{:}\eta^1)\text{-}$ $(\mu_2\text{-}\eta^2\text{:}\eta^1)$-BTB tetradentate and $(\mu_1\text{-}\eta^1\text{:}\eta^0)\text{-}(\mu_1\text{-}\eta^1\text{:}\eta^1)\text{-}(\mu_1\text{-}\eta^1\text{:}\eta^1)\text{-}$ BTB tridentate coordination modes (Fig. S1c and S1d, ESI†). Note that Cd1 and Cd3 are connected together *via* the bridge linking of O11 to form a dinuclear SBU (Fig. S2b, ESI†), which is further joined together by an aqua molecule to extend to an infinite one-dimensional (1D) chain. BTB^{3-} ligands link Cd(II) atoms to form a 3D architecture (Fig. 2b). Furthermore, Cd1 and Cd2 as well as Cd3 and Cd2 are connected by L to form the final 3D framework of **2** (Fig. 2c). PLATON calculation suggests that the resulting free volume after the removal of free water molecules is 16.1%.

To simplify the 3D structure of **2**, topological analysis was performed. As illustrated in Fig. S2b (ESI†), BTB^{3-} ligand, Cd2,

and dinuclear SBU can be treated as 3, 4, and 8 connectors, respectively. Therefore, **2** is an unusual (3, 4, 8)-connected 3-nodal 3D net with the point (Schläfli) symbol of $\{4\cdot6^2\}_2\{4^2\cdot6^3\cdot7\}\{4^4\cdot6^{14}\cdot7^3\cdot8^6\cdot10\}$ (Fig. 2d).

Thermogravimetric analysis (TGA) and powder X-ray diffraction (PXRD)

TGA was performed to investigate the thermal stability of the frameworks, and the results are shown in Fig. S3 (ESI†). The TG curve of **1** shows a weight loss of 12.69% in the temperature range of 30–165 °C, corresponding to the release of free and coordinated water molecules together with the bridging OH groups (calcd 12.54%), and the residue is stable up to about 360 °C. The TG curve of the activated sample of **1** confirms the complete removal of free and coordinated water molecules in the framework, and the loss of 2.67% before 160 °C is may be due to the release of the OH groups (calcd 2.52%). In the case of **2**, a weight loss of 7.75% was observed in the temperature range of 30–160 °C, corresponding to the loss of free and bridging water molecules (calcd 8.50%), and a further weight loss was observed at about 370 °C, corresponding to the collapse of the framework. The TG data of the activated sample of **2** confirms the complete removal of free solvent molecules in the framework. The phase purity of the bulk samples was investigated *via* the PXRD measurements, and each PXRD pattern of the as-synthesized sample was consistent with the simulated pattern (Fig. S4, ESI†), implying the pure phases of **1** and **2**. Fig. S4 (ESI†) also show the PXRD patterns for **1** and **2** after adsorption of the dyes and CO_2/N_2, confirming that the crystalline structures of **1** and **2** are preserved.

Magnetic property of 1

There are tetranuclear SBUs in **1** in which four Co(II) atoms are linked together by two OH$^-$ groups; thus, magnetic interactions may occur inside the tetranuclear SBU. Accordingly, magnetic measurements were carried out for the crystalline sample of **1** in the temperature range of 300–2 K at a field of 1000 Oe. For **1**, the $\chi_m T$ value per Co$_4$ unit is 9.84 cm^3 K mol^{-1} at room temperature, which is higher than the expected value of 7.5 cm^3 K mol^{-1} for four isolated high-spin Co(II) ions with $S = 3/2$ and $g = 2.00$. When the temperature is lowered, the $\chi_m T$ value gradually decreases, and a value of 1.92 cm^3 K mol^{-1} at 2 K is achieved (Fig. 3a). This behavior indicates that **1** exhibits the characteristic predominant antiferromagnetic exchange interactions as well as the spin–orbit coupling effect for the Co(II) ions. The $\chi_m T$–T curve of **1** is similar to that of the helical double-layered compound $[Co_2(OH)(3,4\text{-}PBC)_3]$ as well as $[Me_2NH_2][M_2(bptc)(\mu_3\text{-}OH)(H_2O)_2]$ (M = Co and Ni).[18,19] The corresponding χ_m^{-1} *vs.* T plot obeys the Curie–Weiss law in nature between 300 and 20 K with a Curie constant of $C = 12.621$ cm^3 K mol^{-1} and a Weiss constant of $\theta = -82.50$ K (Fig. 3b). The large negative value of the Weiss constant implies dominating antiferromagnetic coupling within the butterfly-like tetranuclear cluster. Owing to the depopulation of higher Kramers doublets caused by the splitting of the $^4T_{1g}$ ground triplet under the combined action of spin–orbit coup-
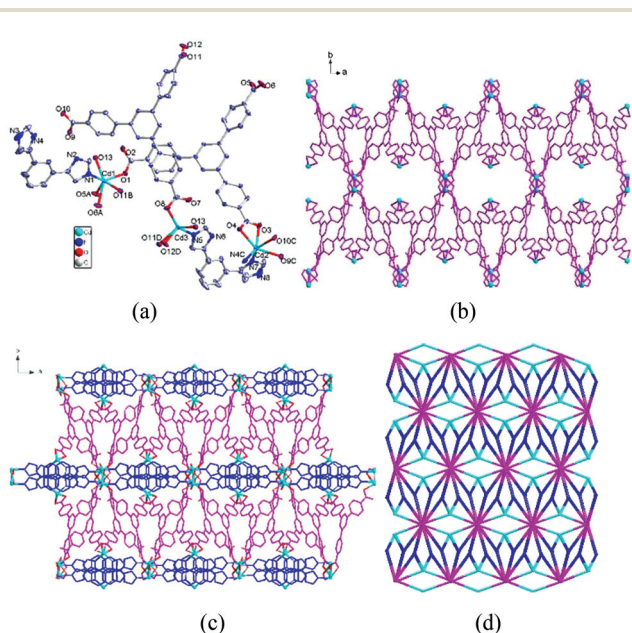
Fig. 2 (a) Coordination environment of Cd(II) in **2** with ellipsoids drawn at the 30% probability level. Hydrogen atoms and free solvent molecules are omitted for clarity. (b) 3D framework of Cd(II)−BTB^{3-}. (c) 3D framework of **2**. (d) Topology of **2**.

(a)

(b)

(c)
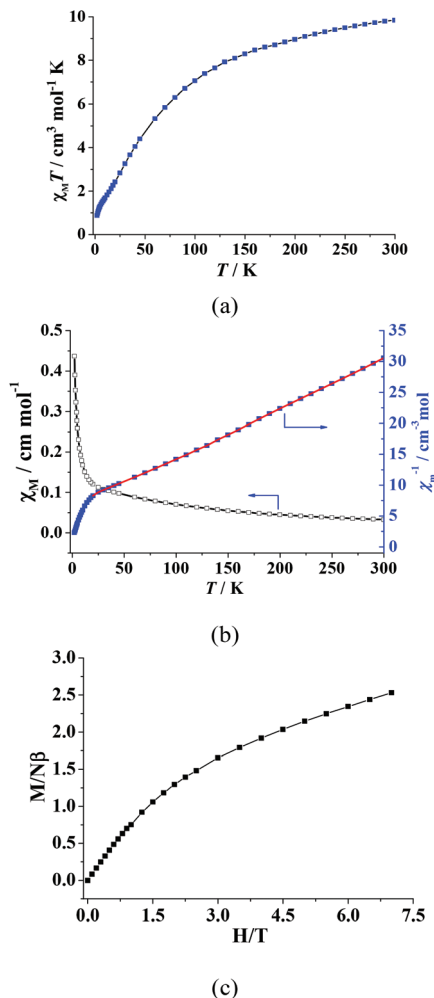
Fig. 3 (a) Magnetic susceptibility data for **1** per Co$_4$ unit presented as plots of $\chi_m T$ versus T under an applied dc of 1000 Oe field. (b) Magnetic susceptibility data for **1**: χ_m^{-1} and χ_m vs. temperature. (c) Field dependence of magnetization for **1** at 1.8 K.
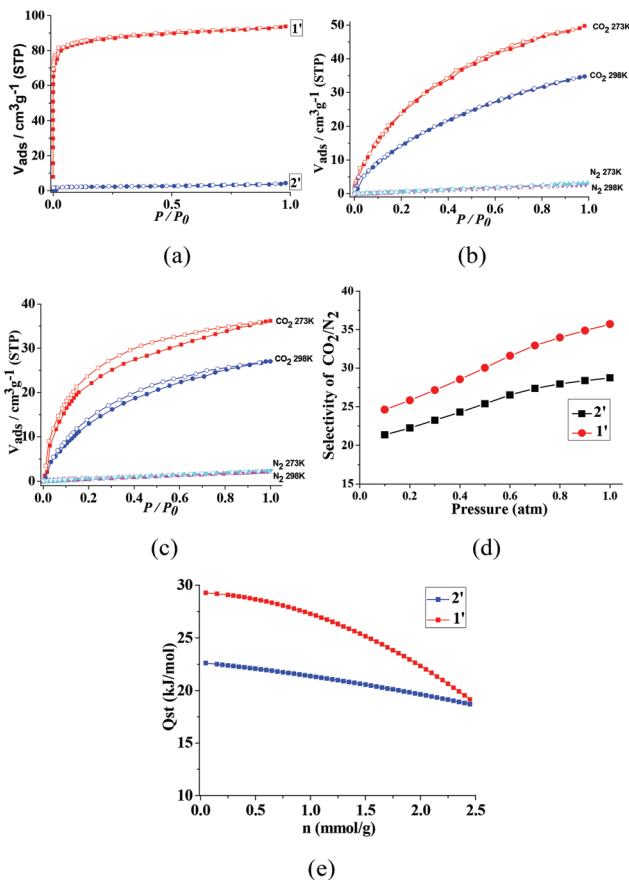

(a)

(b)

(c)

(d)

(e)

Fig. 4 (a) N$_2$ sorption isotherms at 77 K for **1′** and **2′** (filled shape, adsorption; open shape, desorption). (b) N$_2$ and CO$_2$ sorption isotherms at 273 and 298 K for **1′** (filled shape, adsorption; open shape, desorption). (c) N$_2$ and CO$_2$ sorption isotherms at 273 and 298 K for **2′** (filled shape, adsorption; open shape, desorption). (d) IAST-predicted selectivity towards CO$_2$/N$_2$ for **1′** and **2′** at 298 K. (e) The isosteric adsorption enthalpies for **1′** and **2′**.

ling and noncubic crystal field term, single-ion anisotropy of Co(ɪɪ) ions in an octahedral field may also contribute to a negative Weiss constant.[19,20]

The magnetization of **1** slowly and linearly increases with the applied field at 1.8 K, and the field-dependent magnetization at the highest field 7 T is 2.53$N\beta$ (Fig. 3c), far below the saturation value of 12$N\beta$ expected for four spin only Co(ɪɪ) species.

Selective adsorption properties

The TG and PXRD data (Fig. S3 and S4, ESI†) show that **1′** and **2′** (the activated **1** and **2**) maintain their framework structures after the removal of the solvent molecules, *i.e.* they have a permanent porosity. These results encouraged us to examine the adsorption behavior of **1′** and **2′**, and CO$_2$ and N$_2$ gas adsorption experiments were carried out for **1′** and **2′**.

Note that the activated **1**, *i.e.* **1′**, exhibits type-I N$_2$ sorption isotherms at 77 K; however, almost no N$_2$ adsorption was observed for **2′** at 77 K (Fig. 4a). The BET surface area and total

pore volume calculated from the N$_2$ sorption data are 209 m^2 g^{-1} and 0.145 m^3 g^{-1} for **1′**, respectively. A further adsorption study was performed to examine their selective adsorption property at around room temperature. As shown in Fig. 4b and c, at 298 and 273 K, **1′** and **2′** exhibit similar type-I sorption isotherms for CO$_2$, and the adsorption amount of **1′** (34.73 cm^3 g^{-1} at 298 K and 49.77 cm^3 g^{-1} at 273 K at 1 bar) is larger than that of **2′** (27.18 cm^3 g^{-1} at 298 K and 36.18 cm^3 g^{-1} at 273 K at 1 bar). At the same temperature of 298 and 273 K, almost no N$_2$ adsorptions were observed for both **1′** and **2′** (Fig. 4b and c). The results clearly show that **1′** and **2′** can selectively capture CO$_2$ over N$_2$ at 298 and 273 K. The CO$_2$/N$_2$ selectivities were calculated by single-component adsorption isotherms using the Henry's law constants. The selectivities for CO$_2$/N$_2$ were found to be 24.61 (298 K) for **1′** and 21.34 (298 K) for **2′** (Fig. 4d). Comparison of the CO$_2$/N$_2$ selectivity of **1′** and **2′** with those of the reported MOFs suggests that **1′** and **2′** possess good CO$_2$/N$_2$ selectivity under similar conditions: for instance, ZIF-68 (18 at 298 K), ZIF-69 (20 at 298 K), ZIF-70 (17 at 298 K), and ZIF-95 (18 at 298 K).[21] The preferen-

tial and higher affinity for CO_2 as compared to that for N_2 may be instrumental in the CO_2 capture.

The strength of the framework–CO_2 interactions was evaluated by the isosteric heat of adsorption (Q_{st}), calculated *via* the virial method by fitting the adsorption isotherms at 273 and 298 K (Fig. S5, ESI†). The adsorption enthalpy for **1′** is *ca.* 29.3 kJ mol^{-1} and that for **2′** is *ca.* 22.6 kJ mol^{-1} at zero loading (Fig. 4e), which are higher than those of MIL-53(Al) (20.1 kJ mol^{-1}),[22] [Zn$_4$O(TCBPA)$_2$] SNU-77R/SNU-77S/SNU-77H (19.9 to 19.4 kJ mol^{-1}),[23] {Cu$_2$(CPEIP)$_{0.5}$·2H$_2$O} [NJU-Bai13], (21.2 kJ mol^{-1}),[24] and CuBTTri (21 kJ mol^{-1}).[25]

Based on the large channels occupied by the solvent molecules in the frameworks of **1** and **2**, investigations on the guest molecule capture in a solution seems to be promising; accordingly, dye molecule adsorption was studied. We chose different dye molecules, methyl orange (MO), methylene blue (MB), and rhodamine B (RhB, Scheme S1, ESI†), to evaluate the absorption ability of the complexes. As shown in Fig. S6 (ESI†), the standard curves for MO, MB, and RhB were also investigated. The freshly activated samples **1′** and **2′** (10 mg) were immersed in an aqueous solution of MO, MB, and RhB (10 ppm, 20 mL) at room temperature. As a representative, **1′** and **2′** exhibits significant dye removal behavior for methyl orange from aqueous solution, as supported by the time-dependent UV-vis spectra at different time intervals (Fig. 5a and Fig. S7a, Tables S2 and S3, ESI†). For the MB solution, the UV spectra indicate that the concentration of MB decreases with time for the compounds **1′** and **2′** (Fig. 5b and Fig. S7b, Tables S4 and S5, ESI†). In addition, UV-vis results indicate that there are hardly any uptakes as well as color changes for the rose RhB solution (Fig. 5c and Fig. S7c, Tables S6 and S7, ESI†). These facts unambiguously indicated that **1′** and **2′** could actually capture/

adsorb methyl orange dye molecules from an aqueous solution.

The difference in absorption within these three types of dyes may result from the size and shape exclusion because RhB is triangular-planar and relatively large as compared to MO and MB (Scheme S1, ESI†). In addition, absorption may be explained to proceed through multiple interactions such as π–π* stacking/interactions and hydrogen bonding interactions. The results indicate that **1** and **2** could be used as potential adsorbents for dye molecules.[26,27]

Fluorescence sensing property

As is known, MOFs built from d^{10}-configured metal ions and organic ligands may have interesting fluorescent properties; therefore, they can be used as potential sensors for sensing definite molecules.[28] Accordingly, the solid state luminescent properties of the free ligand L as well as **2** were investigated at room temperature. As shown in Fig. S7a (ESI†), intense emission was observed at 381 nm for the free L upon excitation at 340 nm, and an emission band was detected at 379 nm upon excitation (λ_{ex} = 335 nm) for **2**. Compared with that of the free L ligand, the slight blue-shift of the emission of **2** is considered to be caused by the coordination of the ligand to the metal centers.

To examine the potential sensing of the small organic molecules, the fluorescence properties of **2** in different solvent emulsions were investigated for the sensing of small molecules. The stable suspension solutions used for fluorescent measurements were obtained by immersing the powder samples of **2** without activation (5 mg) in a definite solvent (5 ml) and ultrasonicating for 1 h. As shown in Fig. 6a, on comparing the luminescence intensity of **2**, it was observed that CH$_3$CN has a minor effect on the luminescence intensity, whereas others exhibit varying degrees of quenching effect. Particularly, acetone has the most significant influence on the luminescence intensity. The quenching behavior of the acetone molecule might be ascribed to the interaction between C=O of acetone and the framework of **2**.[29]

When the acetone solvent was gradually and increasingly added to **2** dispersed in the CH$_3$CN suspension, the fluorescence intensities of the standard emulsions gradually decreased with the addition of the acetone solvent (Fig. 6b). The fluorescence decrease was nearly proportional to the acetone concentration, and the system ultimately reached the equilibrium state. The decreasing trends of the fluorescence intensity at 335 nm for **2** *versus* the volume ratio of acetone could be fitted with a first-order exponential decay, indicating that fluorescence quenching of **2** using acetone was diffusion-controlled (Fig. S8, ESI†). The results of fluorescence titration of **2** dispersed in CH$_3$CN indicated that a 50% decrease of the luminescene intensity was reached at an acetone content of 1.2 vol%, and almost complete quenching was reached at a concentration of 2.9 vol%. The efficient quenching of acetone in this system can be ascribed to the interaction of the solute and the solvent, which induces the electron transfer from the excited **2** to electron-deficient acetone.[30,31] Furthermore, to
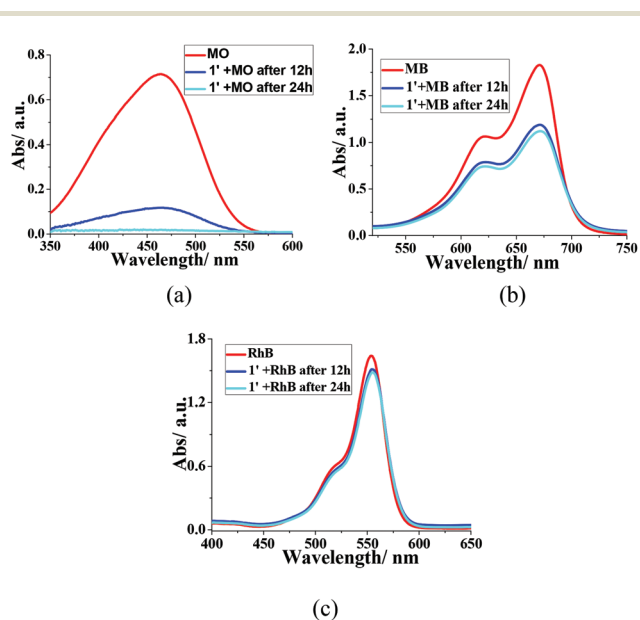

Fig. 5 Adsorption capability of **1′** towards MO (a), MB (b), and RhB (c) (experimental conditions: C_0 (MB): 10 mg L^{-1}, C_0 (MO): 10 mg L^{-1}, adsorbent dose: 10 mg per 20 mL).
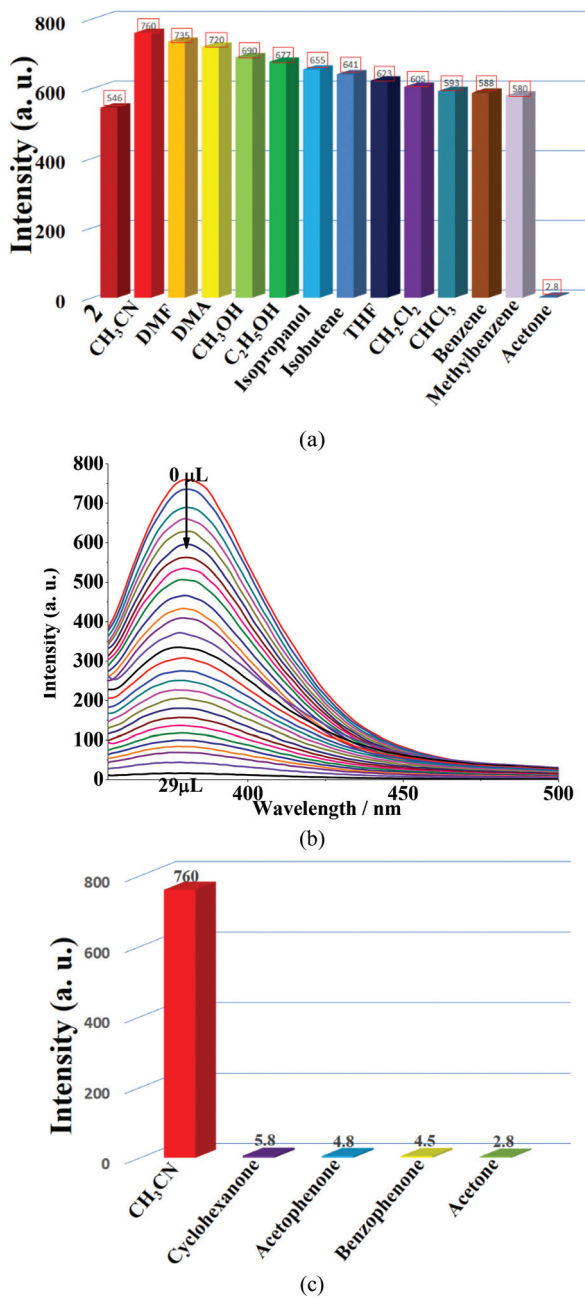
Fig. 6 (a) Photoluminescence intensities of **2** introduced into various pure solvents when excited at 335 nm for **2**. (b) Photoluminescence spectra of **2** dispersed in CH_3CN in the presence of various contents of the acetone solvent (excited at 335 nm). (c) Photoluminescence intensities of **2** introduced into varied ketone molecules when excited at 335 nm.

explore whether the ketone molecule enters the pore or acts on the surface of the framework to cause the fluorescence quenching, **2** was immersed in different ketone molecules, and its fluorescence behavior was examined. As shown in Fig. 6c, the stable suspension of **2** in cyclohexanone, acetophenone, and benzophenone showed highest quenching. The results imply that the interaction between the ketone molecules and the framework of **2** may occur at the surface and cause fluorescence quenching.

Therefore, **2** could be a promising luminescent probe for the detection of small molecules of ketones.

Conclusions

In summary, two porous metal–organic frameworks (MOFs) based on 1,3-di(1*H*-imidazol-4-yl)benzene and 1,3,5-tri(4-carboxyphenyl)benzene were synthesized. Magnetic measurements display that **1** is characteristic of an antiferromagnet. Remarkably, **1** and **2** exhibit relatively high selectivity for the adsorption of CO_2 over N_2 and dye (methyl orange, MO) molecules. Furthermore, **2** may be considered as a potential luminescent probe for the detection of ketone molecules. This study not only provides a novel strategy for the design and synthesis of MOFs but also explores significant potential applications of multifunctional materials.

Acknowledgements

Notes and references

1 (*a*) H. C. Zhou, J. R. Long and O. M. Yaghi, *Chem. Rev.*, 2012, **112**, 673; (*b*) M. Magnetic Kurmoo, *Chem. Soc. Rev.*, 2009, **38**, 1353; (*c*) H. Fu, C. Qin, Y. Lu, Z. M. Zhang, Y. G. Li, Z. M. Su, W. L. Li and E. B. Wang, *Angew. Chem., Int. Ed.*, 2012, **124**, 8109.

2 M. H. Zeng, Z. Yin, Y. X. Tan, W. X. Zhang, Y. P. He and M. Kurmoo, *J. Am. Chem. Soc.*, 2014, **136**, 4680.

3 (*a*) L. D. Kong, R. Y. Zou, W. Z. Bi, R. Q. Zhong, W. J. Mu, J. Liu, R. S. Han and R. Q. Zou, *J. Mater. Chem. A*, 2014, **2**, 17771; (*b*) K. Tang, R. Yun, Z. Lu, L. Du, M. Zhang, Q. Wang and H. Liu, *Cryst. Growth Des.*, 2013, **13**, 1382.

4 (*a*) S. S. Zhao, J. Yang, Y. Y. Liu and J. F. Ma, *Inorg. Chem.*, 2016, **55**, 2261; (*b*) Z. Q. Liu, Y. Zhao, Y. Deng, X. D. Zhang, Y. S. Kang, Q. Y. Lu and W. Y. Sun, *Sens. Actuators, B*, 2017, **250**, 179.

5 (*a*) M. D. Allendorf, C. A. Bauer, R. K. Bhakta and R. J. Houk, *Chem. Soc. Rev.*, 2009, **38**, 1330; (*b*) J. R. Li, R. J. Kuppler and H. C. Zhou, *Chem. Soc. Rev.*, 2009, **38**, 1477.

6 Y. B. Zhang, H. Furukawa, N. Ko, W. Nie, H. J. Park, S. Okajima, bK. E. Deng, H. Cordova, J. Kim and O. M. Yaghi, *J. Am. Chem. Soc.*, 2015, **137**, 2641.

7 S. J. Garibay, Z. Q. Wang, K. K. Tanabe and S. M. Cohen, *Inorg. Chem.*, 2009, **48**, 7341.

8 Z. C. Hu, B. J. Deibert and J. Li, *Chem. Soc. Rev.*, 2014, **43**, 5815.

9 S. S. Chen, M. Chen, S. Takamizawa, M. S. Chen, Z. Su and W. Y. Sun, *Chem. Commun.*, 2011, **47**, 752.

10 S. S. Chen, P. Wang, S. Takamizawa, T. A. Okamura, M. Chen and W. Y. Sun, *Dalton Trans.*, 2014, **43**, 6012.

11 X. L. Zhao and W. Y. Sun, *CrystEngComm*, 2014, **16**, 3247.

12 R. T. Have, M. Huisman, A. Meetsma and A. M. Leusen, *Tetrahedron*, 1997, **53**, 11355.

13 *SAINT, Program for Data Extraction and Reduction*, Bruker AXS, Inc., Madison, WI, 2001.

14 G. M. Sheldrick, *SADABS, Program for Empirical Adsorption Correction of Area Detector Data*, University of Göttingen, Göttingen, Germany, 2003.

15 (*a*) G. M. Sheldrick, *SHELXS-2014, Program for the Crystal Structure Solution*, University of Göttingen, Göttingen, Germany, 2014; (*b*) G. M. Sheldrick, *SHELXL-2014, Program for the Crystal Structure Solution*, University of Göttingen, Göttingen, Germany, 2014.

16 (*a*) A. L. Spek, *Acta Crystallogr., Sect. A: Fundam. Crystallogr.*, 1990, **46**, 194; (*b*) A. L. Spek, *PLATON, A Multipurpose Crystallographic Tool*, Utrecht University, Utrecht, The Netherlands, 2005, or A. L. Spek, *J. Appl. Crystallogr.*, 2003, **36**, 7.

17 A. L. Spek, *Implemented as the PLATON Procedure, A Multipurpose Crystallographic Tool*, Utrecht University, Utrecht, The Netherlands, 1998.

18 J. H. Luo, Y. S. Zhao, H. W. Xu, T. L. Kinnibrugh, D. L. Yang, T. V. Timofeeva, L. L. Daemen, J. Z. Zhang, W. Bao, J. D. Thompson and R. P. Currier, *Inorg. Chem.*, 2007, **46**, 9021.

19 R. X. Yao, X. Xu and X. M. Zhang, *Chem. Mater.*, 2012, **24**, 303.

20 G. X. Wu, H. S. Wu and X. M. Zhang, *Dalton Trans.*, 2010, **39**, 1179.

21 (*a*) R. Banerjee, H. Furukawa, D. Britt, C. Knobler, M. O'Keeffe and O. M. Yaghi, *J. Am. Chem. Soc.*, 2009, **131**, 3875; (*b*) B. Wang, A. P. Cote, H. Furukawa, M. O'Keeffe and O. M. Yaghi, *Nature*, 2008, **453**, 207.

22 S. Couck, J. F. M. Denayer, G. V. Baron, T. Remy, J. Gascon and F. An Kapteijn, *J. Am. Chem. Soc.*, 2009, **131**, 6326.

23 H. J. Park, D. W. Lim, W. S. Yang, T. R. Oh and M. P. Suh, *Chem. – Eur. J.*, 2011, **17**, 7251.

24 Z. Y. Lu, L. T. Du, B. S. Zheng, J. F. Bai and M. X. Zhang, *CrystEngComm*, 2013, **15**, 9348.

25 A. Demessence, D. M. D'Alessandro, M. L. Foo and J. R. Long, *J. Am. Chem. Soc.*, 2009, **131**, 8784.

26 Y. L. Li, Y. Zhao, P. Wang, Y. S. Kang, Q. Liu, X. D. Zhang and W. Y. Sun, *Inorg. Chem.*, 2016, **55**, 11821.

27 (*a*) Y. Han, S. N. Sheng, F. Yang, Y. B. Xie, M. J. Zhao and J. R. Li, *J. Mater. Chem. A*, 2015, **3**, 12804; (*b*) K. Q. Liu, X. Jiang, C. Z. Wang, L. Mei, Z. N. Xie, W. Q. Tao, X. L. Zhang, Z. F. Chai and W. Q. Shi, *Chem. – Eur. J.*, 2017, **23**, 529.

28 (*a*) K. C. Wang, Z. E. Lin, S. Huang, J. Sun and Q. H. Zhang, *Eur. J. Inorg. Chem.*, 2016, 3411; (*b*) Q. Chen, W. Xue, J. B. Lin, Y. S. Wei, Z. Yin, M. H. Zeng, M. Kurmoo and X. M. Chen, *Chem. – Eur. J.*, 2016, **22**, 12088.

29 C. Ma, C. Q. Jiao, Z. G. Sun, Y. Y. Zhu, X. W. Zhang, M. L. Wang, D. Yang, Z. Zhao, H. Y. Li and B. Xing, *RSC Adv.*, 2015, **5**, 79041.

30 F. H. Liu, C. Qin, Y. Ding, H. Wu, K. Z. Shao and Z. M. Su, *Dalton Trans.*, 2015, **44**, 1754.

31 Z. M. Hao, X. Z. Song, M. Zhu, X. Meng, S. N. Zhao, S. Q. Su, W. T. Yang, S. Y. Song and H. J. Zhang, *J. Mater. Chem. A*, 2013, **1**, 11043.